NANOSYSTEMS:
PHYSICS, CHEMISTRY, MATHEMATICS

Original article

Zakharova A.S., et al. *Nanosystems: Phys. Chem. Math.*, 2024, **15** (5), 702–709.
http://nanojournal.ifmo.ru
DOI 10.17586/2220-8054-2024-15-5-702-709

Highly dispersed anti-Stokes phosphors based on KGd_2F_7:Yb,Er single-phase solid solutions

Anna S. Zakharova[1,2,3], Sergey V. Kuznetsov[2], Alexander A. Alexandrov[1,2], Daria V. Pominova[2], Valery V. Voronov[2], Pavel P. Fedorov[2], Vladimir K. Ivanov[1]

[1]Kurnakov Institute of General and Inorganic Chemistry of the Russian Academy of Sciences, Moscow, Russia
[2]Prokhorov General Physics Institute of the Russian Academy of Sciences, Moscow, Russia
[3]National Research University Higher School of Economics, Moscow, Russia

Corresponding author: Anna S. Zakharova, AnyaZakharova2606@mail.ru

PACS 61.46 Df

ABSTRACT The possibility of doping the KGd_2F_7 matrix with ytterbium and erbium ions by introducing yttrium ions with a concentration of 25 mol.% was confirmed and the conditions were determined for the synthesis of anti-Stokes phosphors based on single-phase KGd_2F_7:Yb,Er solid solutions. The dependences were revealed of the sizes of coherent scattering regions, crystal lattice parameters, and energy yield of luminescence on the temperature and duration of heat treatment. Heat treatment conditions were determined to ensure the achievement of intense anti-Stokes luminescence. As a result, effective phosphors KGd_2F_7:Yb (20.0 mol.%),Er (4.0 mol.%) with an energy yield of up-conversion luminescence of 3.80 % were developed. Disordering of the crystal structure (transition from cubic to tetragonal modification) at a temperature of 600 °C was recorded, corresponding to the rule of Ostwald steps.

KEYWORDS inorganic fluorides, anti-Stokes luminescence, KGd_2F_7, co-precipitation technique, ytterbium, erbium

ACKNOWLEDGEMENTS The study was supported by the Russian Science Foundation (grant No. 22-13-00167). The analysis of the composition, structure and properties of the materials obtained was carried out using the equipment of the JRC PMR IGIC RAS.

FOR CITATION Zakharova A.S., Kuznetsov S.V., Alexandrov A.A., Pominova D.V., Voronov V.V., Fedorov P.P., Ivanov V.K. Highly dispersed anti-Stokes phosphors based on KGd_2F_7:Yb,Er single-phase solid solutions. *Nanosystems: Phys. Chem. Math.*, 2024, **15** (5), 702–709.

1. Introduction

Anti-Stokes phosphors based on fluoride matrices doped with lanthanide ions, due to a combination of unique optical properties, are widely used for the anti-counterfeiting labels [1–7], increasing the efficiency of solar panels [8–11], bioimaging [12–15], and *in vivo* nanothermometry [16–21], sorting of plastic waste [22, 23], etc. Currently, the most widely studied matrices are based on β-$NaYF_4$ [12, 24–28], β-$NaGdF_4$ [2, 29, 30], SrF_2 [21, 31–34] and BaF_2 [35]. Solid solutions in the KF–GdF_3 system have been poorly studied [36], but interest in them is due to the fact that matrices based on this system are characterized by lower phonon energy compared to other fluorides, which can lead to an increase in the luminescence quantum yield. One of the key factors determining the efficiency of anti-Stokes luminescence is the size of the coherent scattering regions [29, 30], since it determines the surface/internal volume ratio of crystallites. As a rule, an increase in particle size helps to increase the luminescence intensity. In addition, the effect of the perfection of phosphor particles on the luminescence light output was noted, which manifests itself in the magnitude of microstrains [37]. Thus, optimization of synthesis conditions, including temperature and duration of heat treatment, is an important task to achieve maximum efficiency of anti-Stokes phosphors.

In the present article, we report the results of the investigation of the conditions for the synthesis of anti-Stokes KGd_2F_7:Yb,Er phosphors with a high energy yield and confirm the possibility of doping the KGd_2F_7 matrix with ions of rare earth elements of the yttrium subgroup with a molar concentration of up to 25 %.

2. Materials and methods

The starting materials were: $Gd(NO_3)_3{\cdot}6H_2O$ (99.99 mass %, Lanhit), $Y(NO_3)_3{\cdot}6H_2O$ (99.99 mass %, Lanhit), $Yb(NO_3)_3{\cdot}6H_2O$ (99.99 mass %, Lanhit), $Er(NO_3)_3{\cdot}5H_2O$ (99.99 mass %, Lanhit), $KF{\cdot}2H_2O$ (pure grade, Chemical plant of fluorine salts, Russia), $CH_3CH(OH)CH_3$ (extra-pure grade, Chimmed) and bidistilled water. The content of crystalline hydrate water in rare-earth elements (REE) nitrates was determined using thermogravimetric analysis, calcining

the initial crystalline hydrates of nitrates of rare earth elements to 1000 °C. Based on the results of the analysis, the content of crystalline hydrate water in nitrates was determined: $Gd(NO_3)_3{\cdot}5.8H_2O$, $Y(NO_3)_3{\cdot}10.7H_2O$, $Yb(NO_3)_3{\cdot}5.1H_2O$, $Er(NO_3)_3{\cdot}4.5H_2O$. A series of syntheses of a solid solution of the composition $K(Y_xGd_{1-x})_2F_7$ was carried out according to the reaction:

$$2xY(NO_3)\cdot 10.7H_2O + 2(1-x)Gd(NO_3)_3\cdot 5.8H_2O + 7KF \rightarrow K(Y_xGd_{1-x})_2F_7\downarrow +6KNO_3 + (9.8x+11.6)H_2O.$$

REE nitrates were dissolved in 280 ml of bidistilled water to a concentration of 0.08 M and placed in one 500 ml polypropylene reactor. In the second reactor, potassium fluoride was dissolved in 40 ml of bidistilled water, taken with a 25 % excess in comparison with stoichiometry and a molar concentration of 16.4 M, which was added dropwise to the solutions of rare earth nitrates. The resulting suspension was stirred at room temperature on a magnetic stirrer for 2 hours, followed by decantation of the mother liquor. The precipitate was washed twice to remove unreacted salts with a 9:1 mixture of isopropyl alcohol and bidistilled water. The absence of nitrate ions was confirmed by a qualitative reaction with a 1 % solution of diphenylamine in concentrated sulfuric acid. The precipitate was dried at 45 °C. The mass yield of the reaction was 89 %.

The KGd_2F_7:Yb(20.0 mol.%),Er (4.0 mol.%) phosphors were obtained according to the reaction:

$$1.52Gd(NO_3)_3\cdot 5.8H_2O + 0.40Yb(NO_3)_3\cdot 5.1H_2O + 0.08Er(NO_3)_3\cdot 4.5H_2O + 7KF \rightarrow KGd_{1.52}Yb_{0.40}Er_{0.08}F_7\downarrow +6KNO_3 + 11.216H_2O.$$

The synthesis technique is similar to the technique used to synthesize $K(Y_xGd_{1-x})_2F_7$ solid solutions.

3. Experimental section

The X-ray diffraction patterns were carried out on a Bruker D8 Advance diffractometer with CuKα radiation. The lattice parameters were calculated using the Topas 4.2 software. The sizes of coherent scattering regions were calculated using the DIFFRAC.EVA V2.1 software. Microphotographs were taken on an Amber GMH scanning electron microscope (Tescan, Czech Republic) at an accelerating voltage of 1 kV using a secondary electron detector. To determine the chemical composition of the samples, an Oxford Instruments X-MAX detector with an accelerating voltage of 20 kV was used. The average diameter of the agglomerates was determined in the ImageJ 1.52a program based on 100 particles. Heat treatment temperatures were selected based on differential scanning calorimetry (Netzsch STA 449 F3 Jupiter, Germany) and thermogravimetric analysis (MOM Q-1500 D). The energy yield (EY, %) of anti-Stokes luminescence was determined using a LESA-01 fiber-optic spectrometer (BIOSPEC, Russia) using an integrating sphere (Avantes, the Netherlands). The error in determining the energy yield of anti-Stokes luminescence was 0.02 %.

4. Results and discussion

When producing phosphors, the practically important concentration of the dopant is the doping of rare earth elements up to 25 mol.%, since a further increase leads to concentration quenching and to the multiphase nature of the sample. The use of yttrium makes it possible to simulate any doping of rare earth elements with the yttrium subgroup. In order to confirm the possibility of doping the KGd_2F_7 matrix with ytterbium and erbium ions with concentrations of 20 and 4 mol.%, respectively, a solid solution was synthesized with the nominal composition $KGd_{1.5}Y_{0.5}F_7$. The X-ray diffraction pattern of the synthesized sample is presented in Fig. 1, the results of calculation of the lattice parameters are given in Table 1. When using a stoichiometric amount of KF for the synthesis of a solid solution (Fig. 1a), two-phase samples are formed: a phase based on $KGd_{1.5}Y_{0.5}F_7$ and GdF_3. The formation of GdF_3 is associated with the leaching of potassium by water [38]. The lattice parameters are close to the data on the JCPDS card #00-057-0574 for KGd_2F_7. To prevent potassium leaching, a 25 mol.% excess of KF was used in subsequent syntheses (Fig. 1b), resulting in single-phase samples.

Micrographs of $KY_{0.5}Gd_{1.5}F_7$ sample show spherical agglomerates (Fig. 2a) with an average particle size of 152 nm (Fig. 2b). According to EDX, the sample contains a slightly elevated content of gadolinium ($KY_{0.47}Gd_{1.53}F_7$), which, however, is within the error limits of the chosen method for determining the chemical composition.

As a result, a procedure was determined for the synthesis of single-phase solid solutions $KY_xGd_{1-x}F_7$, in which the concentration of the doping component was 25 mol.%, which proves the possibility of doping the matrix with ytterbium (20 mol.%) and erbium (4 mol.%) ions.

After confirming the possibility of doping the KGd_2F_7 matrix with yttrium ions with a concentration of 25 mol.%, the single-phase anti-Stokes KGd_2F_7:Yb (20.0 mol.%), Er (4.0 mol.%) phosphors were synthesized. Since the synthesis was carried out from the aqueous phase, special attention was paid to determining the heat treatment regimes that ensure the removal of physically and chemically bound water. The presence of water and hydroxyl ions leads to quenching of luminescence [43, 44]. According to differential scanning calorimetry and thermogravimetry, smooth weight loss ($\Delta = 0.09$ wt.%) occurs in steps and ends at a temperature of 340 °C (Fig. 3). An exothermic peak is observed on the DSC curve at a temperature of 600 °C, probably corresponding to a phase transition.

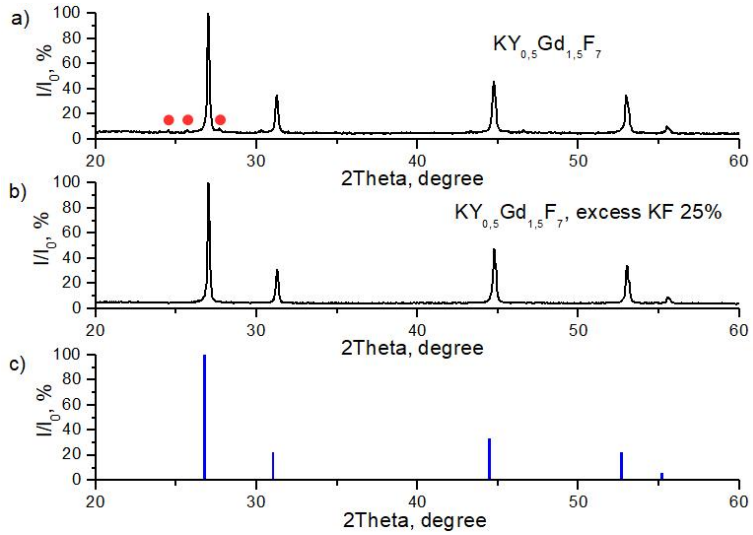

FIG. 1. X-ray diffraction patterns of samples of $KGd_{1.5}Y_{0.5}F_7$ solid solutions: a – $KY_{0.5}Gd_{1.5}F_7$ with a stoichiometric amount of KF; b – $KY_{0.5}Gd_{1.5}F_7$ with a 25 % excess of KF; c – card JCPDS#00-057-0574, corresponding to the KGd_2F_7 phase. The red dot marks the reflections of the GdF_3 phase

TABLE 1. Crystal lattice parameters of $KY_{0.5}Gd_{1.5}F_7$ samples prepared at different potassium fluoride concentrations

Sample code in Fig. 1	Composition	Lattice parameters, Å		Amount of KF
		$K(Y_xGd_{1-x})_2F_7$	GdF_3	
a	$KY_{0.5}Gd_{1.5}F_7$	$a = 5.7366(2)$	$a = 6.6513(91)$ $b = 6.9696(51)$ $c = 4.3790(37)$	Stoichiometric amount of KF
b	$KY_{0.5}Gd_{1.5}F_7$	$a = 5.7337(1)$		25 % Excess of KF
c	KGd_2F_7 JCPDS #00-057-0574	$a = 5.762(2)$		

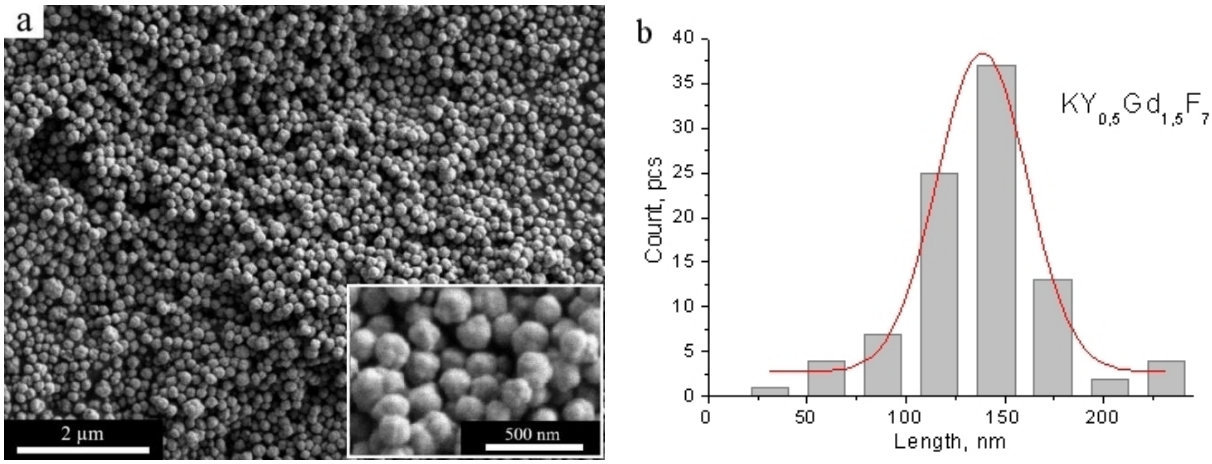

FIG. 2. SEM micrographs (a) and particle size distribution (b) for the sample of $KY_{0.5}Gd_{1.5}F_7$

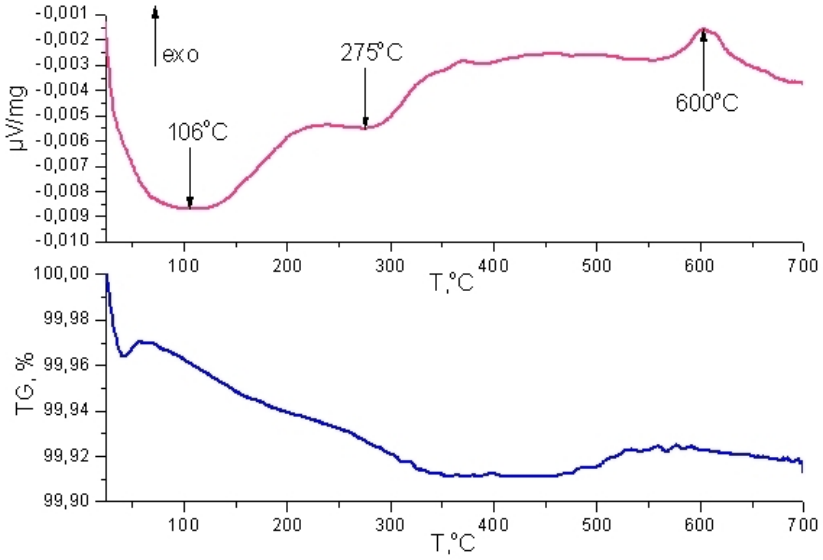

FIG. 3. DSC-TG data for the KGd_2F_7:Yb,Er sample

To identify the nature of the exothermic effect at 600 °C and determine the heat treatment temperature that ensures the production of the most effective phosphors of the composition KGd_2F_7:Yb(20 mol.%), Er(4 mol.%), and taking into account papers [33, 38], we selected the temperatures 500 and 600 °C. The heat treatment of anti-Stokes phosphors was carried out using two methods. In the first case, when the specified temperature was reached, the sample was immediately removed from the oven. In the second case, it was kept at this temperature for 4 hours.

X-ray diffraction patterns of KGd_2F_7:Yb(20 mol.%),Er(4 mol.%) samples after heat treatment at temperatures of 500 and 600 °C with exposure for 0 hours and 4 hours are shown in Fig. 4.

For the samples annealed at 500 °C (0 h) (Fig. 4a) and 500 °C (4 h) (Fig. 4b), the X-ray diffraction patterns correspond to the cubic structure of KGd_2F_7 (JCPDS #00-057-0574) with a slight shift in the X-ray reflections compared to JCPDS #00-057-0574 due to the substitution of gadolinium ions by ytterbium and erbium ions [34], which have smaller radii. After heat treatment at 600 °C (0 h) (Fig. 4d), a change in the crystal structure from cubic to tetragonal is observed, which is completed by heat treatment for 4 h (Fig. 4e). This process is explained by the ordering of the structure according to the Ostwald step rule [40]. Calculations of lattice parameters and coherent scattering regions (CSR) are presented in Table 2.

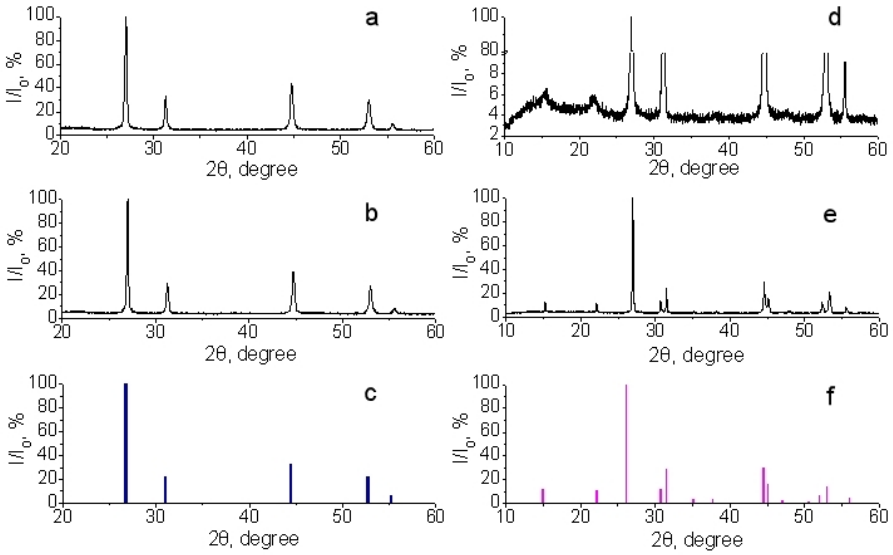

FIG. 4. X-ray diffraction patterns of KGd_2F_7:Yb(20 mol.%),Er(4 mol.%) powders prepared under different heat treatment conditions: a – 500 °C, 0 h; b – 500 °C, 4 h; c – JCPDS #00-057-0754; d – 600 °C, 0 h; e – 600 °C, 4 h; f – X-ray diffraction pattern of sample $K_{0.33}Gd_{0.67}F_{2.33}$ with a tetragonal crystal lattice from the article [39]

TABLE 2. Crystal lattice parameters of KGd_2F_7:Yb (20 mol.%), Er (4 mol.%), samples prepared under different heat treatment conditions

Heat treatment T, °C	Heat treatment duration, h	Sp. group	Lattice parameters, Å	CSR, nm	Composition according to EDX	EY*, %
500	0	*F*m-3m	$a = 5.7341(2)$	47	$KGd_{1.49}Yb_{0.39}Er_{0.07}F_{6.85}$	0.40
500	4	*F*m-3m	$a = 5.7382(2)$	56	$KGd_{1.48}Yb_{0.38}Er_{0.07}F_{6.79}$	0.54
600	0	*P*4/mmm	$a = 4.0630(4)$, $c = 5.7250(6)$	67	$KGd_{1.48}Yb_{0.38}Er_{0.07}F_{6.79}$	1.10
600	4	*P*4/mmm	$a = 4.0242(1)$, $c = 5.8253(3)$	79	$KGd_{1.48}Yb_{0.38}Er_{0.07}F_{6.79}$	3.80
JCPDS #00-057-0574		*F*m-3m	$a = 5.762(2)$			
* [39]		*P*4/mmm	$a = 4.061$, $c = 5.853$			

With increasing temperature and time of heat treatment, a slight increase in lattice parameters and CSR values was revealed. DSC-TG and X-ray diffraction data allow us to conclude that the detected exo-effect at 600 °C corresponds to a change in structure from cubic to tetragonal. The X-ray diffraction pattern retains the main X-ray reflections corresponding to the cubic structure, but additional peaks with lower intensity appear which corresponds to the ordering of the crystal lattice. Note that the equilibrium modification KGd_2F_7 is characterized by a tetragonal system, the crystal lattice of which is derived from the fluorite structure [41].

Scanning electron microscopy data for samples subjected to heat treatment under various conditions confirm the results of DSC-TG and XRD. Rounded agglomerates with an average diameter of about 145 nm are visible in the images of samples annealed at a temperature of 500 °C (Fig. 5a,b). In samples that were annealed at 600 °C a change in morphology is observed with simultaneous sintering of agglomerates to micron size.

According to the results of energy dispersive analysis (Table 2), an overestimation (by 3 %) of the potassium content in all samples was revealed compared to the stoichiometric one. The content of ytterbium and erbium, within the error of the determination method, corresponds to the nominal.

For the KGd_2F_7:Yb (20.0 mol.%), Er (4.0 mol.%) samples, anti-Stokes luminescence spectra were recorded (Fig. 6) and the energy yield was estimated using an integrating sphere (Table 1). In the luminescence spectra, characteristic luminescence bands of erbium are observed in the red and green regions of the spectrum, which correspond to the $^4F_{9/2} \rightarrow {}^4I_{15/2}$ and $^2H_{11/2}, {}^4S_{3/2} \rightarrow {}^4I_{15/2}$ transitions of erbium, respectively. The most intense band was recorded at 670 nm.

The data obtained indicate a significant increase in the efficiency of anti-Stokes luminescence with increasing temperature and time of heat treatment due to an increase in both particle size and ordering of the crystal structure. The highest value of the energy yield of anti-Stokes luminescence (3.80 ± 0.02 %) was recorded for a sample with a tetragonal crystal lattice after annealing for 4 hours at 600 °C. The achieved energy yield of anti-Stokes luminescence is 2.25 times higher than that presented in the literature [33], which is due to the ordering of the crystal structure of the phosphor.

Note that both cubic and tetragonal modifications of KGd_2F_7 should contain clusters of the Gd_6F_{37} type [42] with a size of about 1.5 nm. The close arrangement of Yb/Er cations in these clusters ensures efficient energy transfer and contributes to obtaining a high light output of anti-Stokes luminescence.

5. Conclusion

A single-phase solid solution with a fluorite structural type of composition $KY_{0.5}Gd_{1.5}F_7$ was synthesized by using the co-precipitation from aqueous solutions technique while varying various synthesis parameters. An optimized procedure for the synthesis of a solid solution of the specified composition involves a dropwise addition of 25 % excess potassium fluoride to a solution of rare earth nitrates, followed by washing with a 9:1 mixture of isopropyl alcohol and bidistilled water. Using the proposed method anti-Stokes phosphor powders of KGd_2F_7:Yb(20 mol.%),Er(4 mol.%) were synthesized for which an increase in the sizes of coherent scattering regions, lattice parameters, and energy yield of up-conversion luminescence is observed with increasing duration and temperature heat treatment. The heat treatment temperature (600 °C) has been determined at which ordering of the KGd_2F_7:Yb(20 mol.%),Er(4 mol.%) structure occurs, which consists in a change in the structural type from cubic to tetragonal. The highest energy yield of up-conversion luminescence (3.80 %) was recorded for a sample with a tetragonal crystal lattice (*P*4/*mmm*, $a = 4.024$ Å, $c = 5.825$ Å).

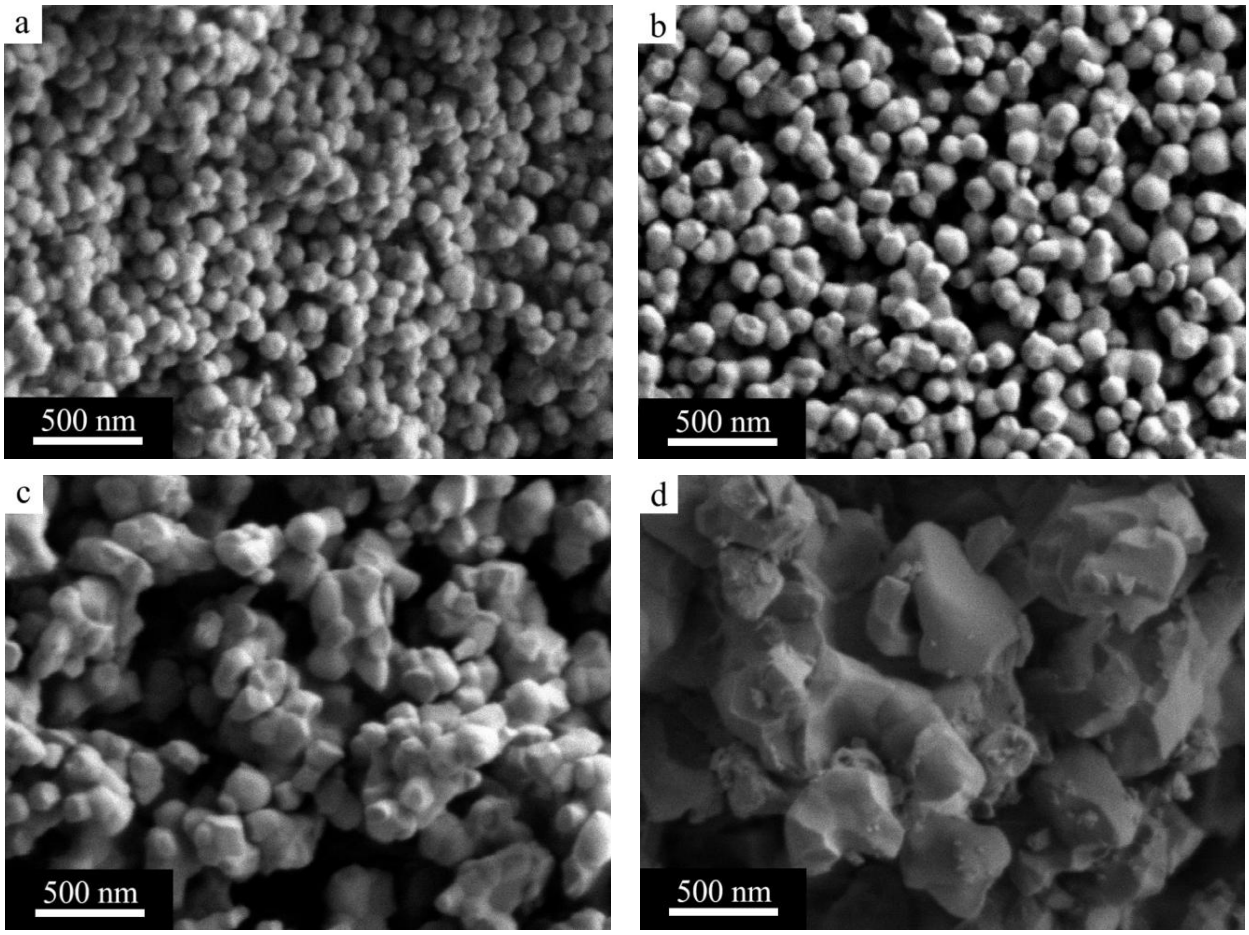

FIG. 5. SEM micrographs of a KGd_2F_7:Yb (20 mol.%),Er(4 mol.%) sample after heat treatment under various conditions: a – 500 °C, 0 h; b – 500 °C, 4 h; c – 600 °C, 0 h; d – 600 °C, 4 h

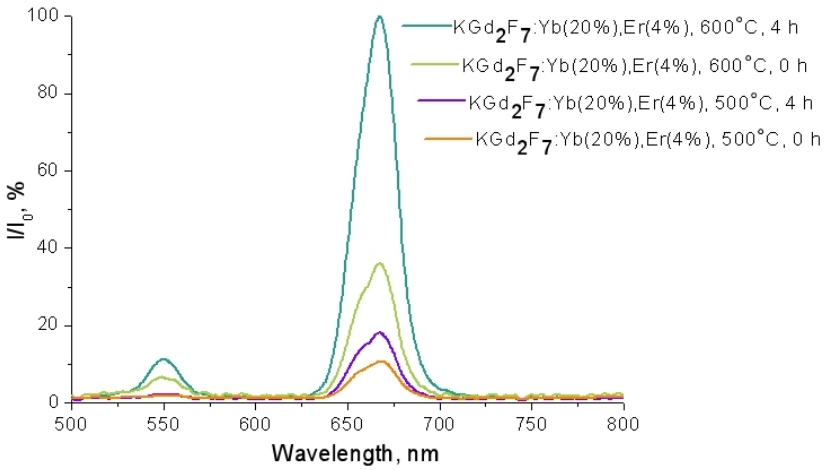

FIG. 6. Luminescence spectra of KGd_2F_7:Yb(20 mol.%),Er(4 mol.%) samples after heat treatment

References

[1] Kumar A., Prakash Tiwari S., Swart H.C., da Silva J.C.G.E. Infrared interceded YF_3:Er^{3+}/Yb^{3+} upconversion phosphor for crime scene and anti-counterfeiting applications. *Optical Materials*, 2019, **92**, P. 347–351.

[2] Maturi F.E., Brites C.D.S., Silva R.R., Nigoghossian K., Wilson D., Ferreira R.A.S., Ribeiro S.J.L., Carlos L.D. Sustainable smart tags two-step verification for anticounterfeiting triggered by the photothermal response of upconverting nanoparticles. *Advanced Photonics Research*, 2021, **3**, #2100227.

[3] Han X., Song E., Zhou B., Zhang Q. Color tunable upconversion luminescent perovskite fluoride with long-/short-lived emissions toward multiple anti-counterfeiting. *J. of Materials Chemistry C*, 2019, **7**, #8226.

[4] Xie S., Gong G., Song Y., Tan H., Zhang C., Li N., Zhang Y., Xu L., Xu J., Zheng J. Design of novel lanthanide-doped core-shell nanocrystals with dual up-conversion and down-conversion luminescence for anti-counterfeiting printing. *Dalton Transactions*, 2019, **48**, P. 6971–6983.

[5] Cui E., Xing G., Yuan X., Zhang Y., Artizzu F., Liao X., Tang J., Zhao Y., Zhao P., Liu K., Liu J. Simultaneously excited downshifting/upconversion luminescence from lanthanide-doped core-shell lead-free perovskite nanocrystals for encryption and data storage. *Advanced Functional Materials*, 2024, **8**, P. 2173–2180.

[6] Suo H., Zhu Q., Zhang X., Chen B., Chen J., Wang F. High-security anti-counterfeiting through upconversion luminescence. *Materials Today Physics*, 2021, **21**, #100520.

[7] Liu J., Rijckaert H., Zeng M., Haustraete K., Laforce B., Vincze L., Van Driessche I., Kaszmaerek A.M., Van Deun R. Simultaneously from lanthanide-doped core/shell fluoride nanoparticles for multimode anticounterfeiting. *Advanced Functional Materials*, 2018, **28**, #1707365.

[8] Huang X. Broadband dye-sensitized upconversion: A promising new platform for future solar upconverter design. *J. of Alloys Compounds*, 2017, **690**, P. 356–359.

[9] Fischer S., Ivaturi A., Jakob P., Kramer K.W., Martin-Rodriges R., Meijerink A., Richards B.S., Golgschmidt J.C. Upconversion solar cell measurements under real sunlight. *Optical Materials*, 2018, **84**, P. 389–395.

[10] Ghazy A., Safdar M., Lastusaari M., Savin H., Karppinen M. Advances in upconversion enhanced solar cell performance. *Solar Energy and Solar Cell*, 2021, **320**, #111234.

[11] Fisher S., Favilla E., Tonelli M., Goldschmidt J.C. Record Efficient upconverter solar cell devices with optimized bifacial silicon solar cells and monocrystalline $BaYF_8$:30%Er^{3+} upconverter. *Solar Energy Materials and Solar Cell*, 2015, **136**, P. 127–134.

[12] Wang F., Banerjee D., Liu Y., Chen X., Liu X. Upconversion nanoparticles in biological labeling, imaging, and therapy. *Analyst*, 2010, **135**, P. 1839–1854.

[13] Liu Q., Feng W., Li F. Water-soluble lanthanide upconversion nanophosphors: Synthesis and bioimaging applications in vivo. *Coordination Chemistry Reviews*, 2014, **273**, P. 100–110.

[14] Tse W.H., Chen L., McCurdy C.M., Tarapaski C.M., Chronik B.A., Zhang J. Development of biocompatible $NaGdF_4$:Er3+,Yb3+ upconversion nanoparticles used as contrast agents for bio-imaging. *The Canadian J. of Chemical Engineering*, 2019, **97**, P. 2678–2684.

[15] Min Y., Li J., Liu F., Padmanabhan P., Yeow E.K.L., Xing B. Recent advance of biological molecular imaging based on lanthanide-doped upconversion-luminescent nanomaterials. *Nanomaterials*, 2014, **4**, P. 129–154.

[16] Du P., Luo L., Huang X., Yu J.S.. Ultrafast synthesis of bifunctional Er3+/Yb3+-codoped NaBiF4 upconverting nanoparticles for nanothermometer and optical heater. *J. of Colloid and Interface Science*, 2018, **514**, P. 172–181.

[17] Du P., Luo L., Yu J.S. Low-temperature thermometry based on upconversion emission of Ho/Er-codoped $Ba_{0.77}Ca_{0.23}TiO_3$ ceramics. *J. of Alloys and Compounds*, 2015, **632**, P. 73–77.

[18] Zhou S., Jiang S., Wei X., Chen Y., Duan C.-K., Yin M. Optical thermometry based on upconversion luminescence in Yb^{3+}/Ho^{3+} co-doped $NaLuF_4$. *J. of Alloys and Compounds*, 2014, **588**, P. 654–657.

[19] Suo H., Zhao X., Zhang Z., Li T., Goldys E.M., Guo C. Constructing Multiform Morphologies of YF: Er3+/Yb3+ Up-conversion Nano/Microcrystals towards Sub-tissue Thermometry. *Chemical Engineering J.*, 2017, **313**, P. 65–73.

[20] Manciniak L., Prorok K., Frances-Soriano L., Perez-Prieto J., Bernarkiewicz A. A broadening temperature sensitivity range with a core-shell YbEr@YbNd double ratiometric optical nanothermometer. *Nanoscale*, 2016, **8**, P. 5037–5042.

[21] Ryszczynska K., Trejgis K., Marciniak L., Grzyb T. Upconverting SrF_2:Er^{3+} Nanoparticles for Optical Temperature Sensors. *Applied Nano Materials*, 2021, **4**, P. 10438–10448.

[22] Woidsky J., Sander I., Schau A., Moesslein J., Wendler P., Wacker D., Gao G., Kirchenbauer D., Kumar V., Busko D., Howard I.A., Richards B.S., Turshakov A., Wiethoff S., Lang-Koetz C. Inorganic fluorescent marker materials for identification of post-consumer plastic packaging. *Resources, Conservation and Recycling*, 2020, **161**, #104976.

[23] Howard I.A., Busko D., Gao G., Wendler P., Madirov E., Turshakov A., Moesslein J., Richards B.S. Sorting plastics for a circular economy: Perspectives for lanthanide luminescent markers. *Resources, Conservation and Recycling*, 2024, **205**, #107557.

[24] Wang F., Deng R., Liu X.. $NaYF_4$:Yb,Er/$NaYF_4$ Core/Shell Nanocrystals with High Upconversion Luminescence Quantum Yield. *Nature Protocols*, 2014, **9**, P. 1634–1644.

[25] Klier D.T., Kumke M.U. Upconversion Luminescence Properties of $NaYF_4$:Yb:Er Nanoparticles Codoped with Gd^{3+}. *The J. of Physical Chemistry C*, 2015, **119**, P. 3363–3373.

[26] He L., Zou X., He X., Lei F., Jiang N., Zheng Q., Xu C., Liu Y., Lin D. Reducing Grain Size and Enhancing Luminescence of $NaYF_4$:Yb^{3+},Er^{3+} Upconversion Materials. *Crystal Growth and Design*, 2018, **18**, P. 808–817.

[27] Yi G. Synthesis of Hexagonal-Phase $NaYF_4$:Yb,Er and $NaYF_4$:Yb,Tm Nanocrystals with Efficient Up-Conversion Fluorescence. *Advanced Functional Materials*, 2006, **16**, P. 2324–2329.

[28] Wang L., Li Y. Controlled Synthesis and Luminescence of Doped $NaYF_4$ Nanocrystals. *Chemistry of Materials*, 2007, **19**, P. 727–734.

[29] Cheng Q., Sui J., Cai W. Enhanced upconversion emission in Yb^{3+} and Er^{3+} codoped $NaGdF_4$ nanocrystals by introducing Li^+ ions. *Nanoscale*, 2012, **4**, P. 779–784.

[30] Maurya S.K., Kushawaha R., Tiwari S.P., Kumar A., Kumar K., Esteves da Silva J.C.G. Thermal decomposition mediated Er3+/Yb3+ codoped $NaGdF_4$ upconversion phosphor for optical thermometry. *Materials Research Express*, 2019, **6**, #086211.

[31] Saleta Reig D., Grauel B., Konyushkin V.A., Nakladov A.N., Fedorov P.P., Brusko D., Howard I.A., Richards B.S., Resch-Genger U., Kuznetsov S.V., Turshakov A., Wurth C. Upconversion properties of SrF_2:Yb3+,Er3+ single crystals. *J. of Materials Chemistry C*, 2020, **8**, P. 4093–4101.

[32] Pak A.M., Ermakova J.A., Kuznetsov S.V., Ryabova A.V., Pominova D.V., Voronov V.V. Efficient visible range SrF_2:Yb:Er^- and SrF_2:Yb:Tm-based up-conversion luminophores. *J. of fluorine chemistry*, 2017, **194**, P. 16–22.

[33] Rozhnova Yu.A., Kuznetsov S.V., Luginina A.A., Voronov V.V., Ryabova A.V., Pominova D.V., Ermakov R.P., Usachev V.A., Kononenko N.E., Baranchikov A.E., Ivanov V.K., Fedorov P.P. New $Sr_{1-x-z}R_x(NH_4)_zF_{2+x-z}$ (R=Yb, Er) solid solution as precursor for high efficiency upconversion luminophor and optical ceramics on the base of strontium fluoride. *Materials Chemistry and Physics*, 2016, **172**, P. 150–157.

[34] Ermakova J.A., Madirov E.I., Fedorov P.P., Alexandrov A.A., Kuznetsov S.V. Effect of the fluorinating agent type (NH_4F, NaF, KF) on the particle size and emission properties of SrF_2:Yb:Er luminophores. *Mat. Chem. C*, 2024, **12**, P. 1406–1411.

[35] Madirov E., Kuznetsov S.V., Konyushkin V.A., Nakladov A.N., Fedorov P.P., Bergfeldt Th., Hudry D., Busko D., Howard I.A., Richards B.S., Turshtov A. Effect of Yb3+ and Er3+ concentration on upconversion luminescence of co-doped BaF_2 single crystals. *J. Mater. Chem. C*, 2021, **9**, P. 3493–3503.

[36] Karbowiak M., Mech A., Bednarkiewicz A., Strek W. Structural and luminescent properties of nanostructured $KGdF_4:Eu^{3+}$ synthesised by coprecipitation method. *J. Alloys Comp.*, 2004, **380**, P. 321–326.

[37] Alexandrov A.A., Mayakova M.N., Kuznetsov S.V., Voronov V.V., Pominova D.V., Ivanov V.K., Fedorov P.P. Effect of Structural Perfection of Crystalline β-$NaYF_4$:Er3+,Yb3+ Phosphor Powders on the Efficiency of Their Upconversion Luminescence. *Inorganic Materials*, 2022, **58** (1), P. 90–96.

[38] Zakharova A.S., Alexandrov A.A., Pominiva D.V., Fedorov P.P., Kuznetsov S.V., Ivanov V.K. Synthesis of KGd_2F_7:Yb:Er luminophores by co-precipitation from aqueous solutions. *J. of Structural Chemistry*, 2024, **65**, P. 138–148.

[39] Gredin P., Labeguerie J., Pierrard A., Vaulay M.-J., de Kozak A.R.D. Synthesis and structural characterization of $K_{0.33}Gd_{0.67}F_{2.33}(KGd_2F_7)$ and $K_{0.31}Gd_{0.69}F_{1.84}O_{0.27}$. *Solis State Science*, 2004, **6**, P. 1221–1228.

[40] Ostwald W. Studien über die Bildung und Umwandlung fester Körper. *Zeitschrift für Physikalische Chemie*, 1897, **22**, P. 289–330.

[41] Fedorov P.P. Systems of alkali and rare-earth metal fluorides. *Russian J. Inorg. Chem.*, 1999, **44** (11), P.1703–1727.

[42] Le Fur Y., Aleonard S., Gorius M.F., Roux M.T. Structure crystalline de $K_{0.265}Gd_{0.735}F_{2.47}$. *Z. Krist.*, 1988, **182**, P. 281–290.

[43] Timofeeva E., Orlovskaya E., Popov A., Shaidulin A., Kuznetsov S., Alexandrov A., Uvarov O., Vainer Y., Silaev G., Rähn M., Tamm A., Fedorenko S., Orlovskii Y. The Infuence of Medium on Fluorescence Quenching of Colloidal Solution of the Nd3+:LaF_3 Nanoparticles Prepared with HTMW treatment. *Nanomaterials*, 2022, **12**, 3749.

[44] Fedorov P.P., Kuznetsov S.V., Osiko V.V. Elaboration of Nanofluorides and Ceramics for Optical and Laser Applications. *Photonic and Electronic Properties of Fluoride Materials*, 2016, P. 7–31.

Submitted 29 August 2024; accepted 26 September 2024

Information about the authors:

Anna S. Zakharova – Kurnakov Institute of General and Inorganic Chemistry of the Russian Academy of Sciences, Moscow, Russia; Prokhorov General Physics Institute of the Russian Academy of Sciences, Moscow, Russia; National Research University Higher School of Economics, Moscow, Russia; ORCID 0000-0003-0976-5192; AnyaZakharova2606@mail.ru

Sergey V. Kuznetsov – Prokhorov General Physics Institute of the Russian Academy of Sciences, Moscow, Russia; ORCID 0000-0002-7669-1106; kouznetzovsv@gmail.com

Alexander A. Alexandrov – Kurnakov Institute of General and Inorganic Chemistry of the Russian Academy of Sciences, Moscow, Russia; Prokhorov General Physics Institute of the Russian Academy of Sciences, Moscow, Russia; ORCID 0000-0001-7874-7284; alexandrov1996@yandex.ru

Daria V. Pominova – Prokhorov General Physics Institute of the Russian Academy of Sciences, Moscow, Russia; ORCID 0000-0002-3634-8709; pominovadv@gmail.com

Valery V. Voronov – Prokhorov General Physics Institute of the Russian Academy of Sciences, Moscow, Russia; ORCID 0000-0001-5029-8560; voronov@lst.gpi.ru

Pavel P. Fedorov – Prokhorov General Physics Institute of the Russian Academy of Sciences, Moscow, Russia; ORCID 0000-0002-2918-3926; ppfedorov@yandex.ru

Vladimir K. Ivanov – Kurnakov Institute of General and Inorganic Chemistry of the Russian Academy of Sciences, Moscow, Russia; ORCID 0000-0003-2343-2140; van@igic.ras.ru

Conflict of interest: the authors declare no conflict of interest.